Sol–gel fabrication of thick multilayers applied to Bragg reflectors and microcavities

Sébastien Rabaste, Joël Bellessa, Charles Bovier, Arnaud Brioude, Jean Claude Plénet, Roger Brenier, Olivier Marty, Jacques Mugnier, Jean Dumas

Sol–gel fabrication of thick multilayers applied to Bragg reflectors and microcavities

S. Rabaste[a,*], J. Bellessa[a], A. Brioude[a], C. Bovier[a], J.C. Plenet[a], R. Brenier[a], O. Marty[b], J. Mugnier[c], J. Dumas[a]

[a]*Département de Physique des Matériaux, Université Claude Bernard Lyon1, CNRS-UMR 5586, 43 Boulevard du 11 Novembre, 69622 Villeurbanne Cedex, France*
[b]*Laboratoire d'Electronique, Nanotechnologie et Capteurs, Université Claude Bernard Lyon1, 43 Boulevard du 11 Novembre, 69622 Villeurbanne Cedex, France*
[c]*Laboratoire de Physico-Chimie des Matériaux Luminescents, Université Claude Bernard Lyon1, CNRS-UMR 5620, 43 Boulevard du 11 Novembre, 69622 Villeurbanne Cedex, France*

We discuss attractive potentialities of the sol–gel process applied to planar microcavities with distributed Bragg reflectors (DBRs). This method is well known for its good flexibility and the optical quality of the thin films obtained. The DBRs are composed of alternated TiO_2 and SiO_2 thin films. One of the main problems of the sol–gel process is the stresses induced during the layers heat treatment leading to defects and cracks in the films. The study of these stresses shows that with the appropriate annealing temperature and duration of the firing process, the stress in the SiO_2 layers partially compensates the stress in the TiO_2 layers. DBRs and microcavities formed by 60 stacked layers have been elaborated in these conditions. The reflectivity of such sol–gel DBRs reaches 99.7%. The sol–gel DBRs are used to fabricate microcavities containing Eu^{3+} rare earth ions with a quality factor of approximately 1000.

Keywords: Titanium oxide; Silicon oxide; Multilayers; Optical properties

1. Introduction

Purcell in 1946 [1] has shown that it is possible to modify the spontaneous rate emission of an excited atom if it is inserted in a cavity. Fabry–Perot microcavities are the simplest devices producing this effect. The cavity effects on the emitters are directly correlated to the mirror efficiency [2]. Distributed Bragg reflectors (DBRs) are very often used due to their high reflectivity. Recently, we have shown that cavities with quality factor greater than 10^3 can be fabricated by a sol–gel process [3]. The main advantage of this method is the large variety of emitting materials which can be included homogeneously in the sol–gel layers: rare earth ions, organic molecules, semiconductor nanocrystals. DBRs are constituted of alternated high and low index quarter wave layers. To increase the reflection coefficient, the index contrast between the two materials has to be as large as possible, TiO_2 and SiO_2 which exhibit a refractive index of approximately 2.20 and 1.45, respectively at 650 nm, have been chosen, and the number of layers must be as high as possible. This last condition requires a special elaboration procedure and a careful study of each layer's properties (stresses in the films, crystallization). This control is necessary to obtain crack-free good optical quality sol–gel stacked films for high reflectivity DBRs fabrication.

In this paper, the sol–gel fabrication procedure is described and each material behavior is studied. In the first part, we will expose the sol–gel process for DBRs and microcavities elaboration, the second part will be devoted to the study and measurement of stresses in the

*Corresponding author. Tel.: +33-4-72432987; fax: +33-4-72432987.
E-mail address: sebastien.rabaste@dpm.univ-lyon1.fr (S. Rabaste).

materials. In the third part a TEM study of the layers is presented and finally, the optical properties of microcavities are presented.

2. Sol–gel DBRs fabrication

Thin films constituting the DBRs have been fabricated using a sol–gel method. The sol–gel process is based on a chemical transformation of liquid alkoxide precursors into solid state products by hydrolysis and polymerization reactions at room temperature. To obtain a good refractive index contrast in the DBRs structure, TiO_2 and SiO_2 materials have been used. The TiO_2 sol was prepared by mixing titanium isopropoxyde and propanol-2. Acetic acid was added to prevent the precipitation of TiO_2 by complexing the titanium alcoxide. Methanol was then used to adjust the viscosity of the sol which controls the thickness of the deposited layer [4]. The solution obtained was transparent and stable during the coating operations. For SiO_2 sol preparation, tetra ethyl ortho silicate (TEOS) is mixed with chloric acid (0.022 molar), and diluted in ethanol (1; 0.0018; 7.55 cm^3) [5]. Films were deposited by a dip coating method under controlled air humidity onto optically polished silicon wafers. The substrates are immersed into the solution and withdrawn from the bath at a constant rate of 6 and 8 cm min^{-1} for TiO_2 and SiO_2, respectively. After each layer deposition, the films were dried at 80 °C for 5 min to evaporate the more volatile solvents and annealed at 350 °C to burn out the organic residues. A very short firing (2 s) at 900 °C is achieved after each deposition of SiO_2 layer. This step is essential for the sol–gel DBRs fabrication and will be detailed in Sections 3 and 4. The samples have been fired using a rapid thermal annealing (RTA) furnace (JIPELEC-JetFirst 100).

Two types of stacked film samples have been performed: simple DBRs and Eu^{3+} doped microcavities. DBRs are made up by alternative depositions of quarter wavelength layers of SiO_2 and TiO_2. The cavities are formed by a half wavelength Eu^{3+} doped SiO_2 layer inserted between two DBRs constituted by seven pairs of quarter wavelength alternated layers. The Eu^{3+} doped active layer is obtained by adding $Eu(NO_3)_3$ into the SiO_2 sol, the molar ratio $Eu(NO_3)_3/Si$ equals 0.02. Two dip coating operations of the same material are necessary to get the quarter wavelength thickness.

3. Stress studies

The formation of cracks and defects in the layers with increasing layer thickness is a well-known problem in the sol–gel procedure [6]. In our case, a conventional annealing treatment, between 300 °C and 700 °C, does not allow the deposition of more than 10 layers without a cracking effect, and more than 30 layers are necessary to fabricate good quality DBRs or optical cavities. Cracks are observed in the films when the stresses exceed the strength of the film. Several effects contribute to these stresses: the structural modification such as densification of the layers and solvent evaporation during the thermal treatment, and the difference of thermal expansion coefficients between the deposited materials and the substrate (2.6×10^{-6} °C^{-1}; 0.5×10^{-6} °C^{-1}; 0.32×10^{-6} °C^{-1} for Si, SiO_2 and TiO_2, respectively). To increase the thickness of the stack, stress evolution in the SiO_2 and TiO_2 films has to be studied as a function of annealing temperature. The stress in the thin films has been measured at room temperature using a H-line bench. In this experiment, the film is deposited on a 100 μm thick silicon substrate. The film's stresses induce a substrate deformation and its curvature radius is optically measured [7]. The integrated stresses which is the stresses value multiplied by the film thickness is deduced from this radius using Stoney's relation [8]

$$\sigma\mathrm{int} = \frac{E.t_s^2}{6(1-\gamma)} * \left(\frac{1}{R} - \frac{1}{R_o}\right) \quad (1)$$

where E is the silicon substrate Young's modulus ($E = 16.5\times10^{10}$ N/m^2), γ is the silicon Poisson's modulus ($\gamma = 0.27$) [9], t_s the substrate thickness, R_o is the radius of curvature of the substrate and R is the radius of curvature of the substrate with the deposited layer.

Two samples have been studied with this technique, the first is a TiO_2 monolayer which was 50 nm thick after an annealing treatment at 200 °C, deposited on a 0.1 mm thick silicon wafer and the second was a 65 nm thick SiO_2 monolayer after annealing treatment at 200 °C, deposited on the same kind of substrate. Each sample had been successively annealed for 15 min between 200 °C and 1050 °C by steps of 100 °C until 800 °C, then by steps of 50 °C. After each step, stress measurements were conducted at room temperature. An uncovered silicon wafer had been heat-treated using the same thermal procedure and no curvature change was observed. Fig. 1 shows the integrated stresses as a function of the annealing temperature for both samples deduced from the radius of curvature measurements. Between 200 °C and 400 °C, the tensile stresses increase for both materials. This stress variation was probably due to the films porosity decrease and the layer densification. After 400 °C and up to 900 °C, the TiO_2 stress remained roughly constant, and for temperatures greater than 900 °C increased rapidly. The SiO_2 layers behavior was drastically different. After 400 °C the stress decreased and changed from tensile to compressive at 800 °C. The main reason which could explain the SiO_2 stress evolution is the difference of thermal expansion coefficient between the substrate and the SiO_2 layer. The thermal coefficient of silicon (2.6×10^{-6} °C^{-1}) is greater than the SiO_2 one (0.5×10^{-6} °C^{-1}) and a

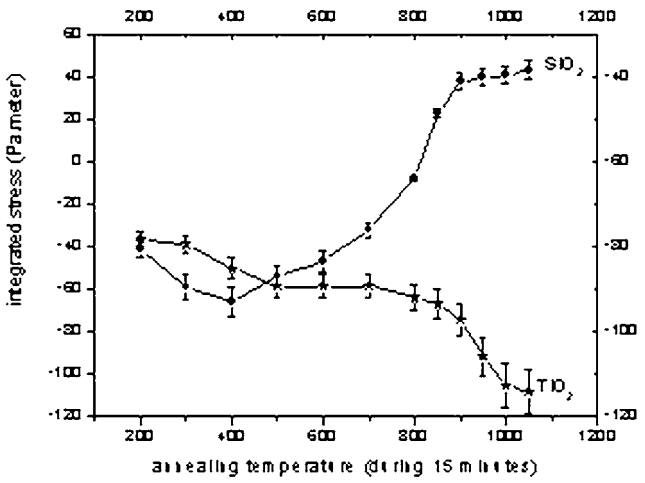

Fig. 1. Variation of the integrated stresses for SiO_2 (circles line) and TiO_2 (stars line) on a Si substrate, vs. the annealing temperature. The precision on the stress value is mainly limited by the uncertainty of the radius measurement and the thickness of the substrate.

compressive stress is induced in the sample proportional to the annealing temperature[10]. The stress measured is the sum of the thermal contribution and the intrinsic stress due to the material formation. When the temperature increases, the compressive thermal stress increases and the tensile intrinsic stress decreases in SiO_2 due to a viscoelastic relaxation, as shown by Fitch et al. [11], leading to a compressive stress for high temperatures.

For temperatures greater than 800 °C the stresses in the TiO_2 and SiO_2 layers are opposed and when these two materials are alternatively stacked, the SiO_2 compressive stress partially compensates the TiO_2 tensile stress. The appropriate temperature to have the best compensation is 900 °C. This temperature has been selected to fabricate the DBRs, and allows a stack of more than 60 layers without any cracks.

4. Material characterization

TiO_2 sol−gel layers start to crystallize at an annealing temperature greater than 350 °C [12]. The crystallites growth in the layer can drastically reduce the optical quality by diffusing the light or creating roughness at the interfaces between the SiO_2 and TiO_2 films in the stack. To observe the TiO_2 crystallization, TEM microscopy has been performed using a TOPCON EM-002B operating at 200 kV. As the annealing temperature was fixed at 900 °C (see Section 2) the only way to modify the crystallites size was to reduce the firing time. Fig. 2a−c show TEM images of three TiO_2 monolayers annealed at 900 °C for 1 min, 10 min and 60 min, respectively. The three layers are fully crystallized and diffraction patterns show that the TiO_2 phase is anatase. The crystallites diameter distribution has been deduced from these images. The mean crystallite diameter and the size distribution increases with the annealing time, due to the crystallites growth, these mean diameters are 45 nm, 75 nm and 91 nm for annealing time of 1 min, 10 min and 60 min, respectively. The crack-free DBRs fabrication process requires a 900 °C annealing step after each SiO_2 layer deposition and the maximal number of SiO_2 layers deposited is 30, corresponding to a total number of stacked layers of 60. An annealing time of 2 s for each SiO_2 layer leads to a total 900 °C annealing time for the first deposited TiO_2 layers always lower than one minute. In this case the TiO_2 crystallite size is smaller than 45 nm and prevents strong Rayleigh scattering [13]. The SiO_2 is still amorphous at this annealing temperature.

Fig. 3 represents a TEM image of a microcavity cross section. The sample preparation has been discussed in [12]. The microcavity is composed of an Eu^{3+} doped SiO_2 layer between two Bragg mirrors, constituted by seven TiO_2/SiO_2 doublets. The total number of layers stacked to fabricate this cavity is 60. The thickness of

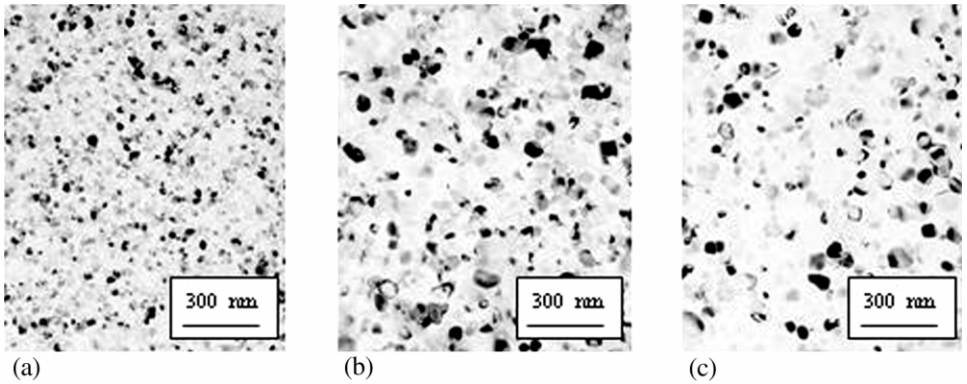

Fig. 2. TEM images of three layers annealed at 900 °C for 1 min (a), 10 min (b), 60 min (c). The mean diameters of the crystals are 45 nm, 75 nm and 91 nm, respectively.

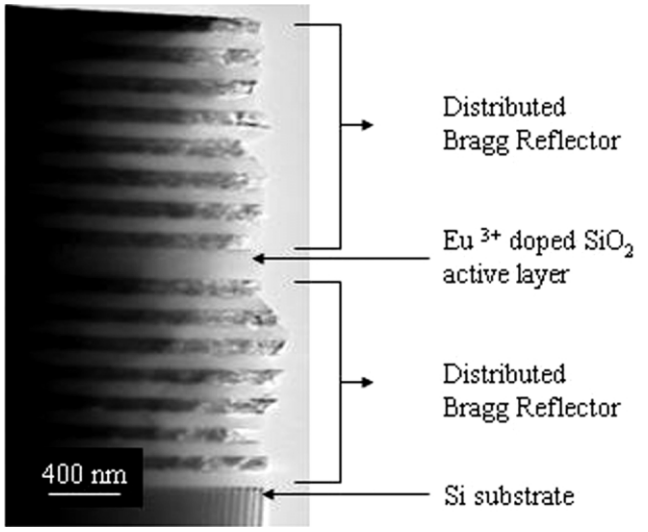

Fig. 3. TEM image of a microcavity cross section. Each DBR is fabricated with seven pairs of alternated layers of SiO_2 (bright layers) and TiO_2 (dark layers), the active layer is a Eu^{3+} doped SiO_2 layer.

each SiO_2 and TiO_2 layer measured on the image is 88 nm and 82 nm, respectively, and the Eu^{3+} doped SiO_2 layer thickness is approximately 170 nm. From Fig. 3, for both materials the thickness fluctuation from one layer to the other is estimated at ± 2 nm. Fig. 4 shows an enlarged image of the cavity of Fig. 3. The interfaces are well defined showing that no mixing or diffusion between the different stacked materials occurs. The crystallization of TiO_2 appears but doesn't introduce observable roughness at the interfaces with the SiO_2 layer.

5. Optical studies

The reflectance spectrum of a 7 doublets DBRs is shown on Fig. 5. This spectrum was measured using a lambda 900 Perkin–Elmer spectrophotometer with a reflection angle of 3°. The reflection band lies between 580 nm and 780 nm and the maximum reflectivity is higher than 99%. A reflection spectrum calculated with a transfer matrix method [14] is drawn in a continuous line and is in fair agreement with the experimental result. The optical indices, used for the simulation, were measured using spectroscopic ellipsometry. The thicknesses deduced from the calculation are 85 nm and 91 nm for TiO_2 and SiO_2, respectively. These values are greater than the TEM measured values; two main reasons explain these differences: the thicknesses variations depending on the sample region studied and the microscopy imprecision. Indeed, TEM observations are made on a cleaved sample. The shape of this sample obliged us to work with TEM conditions far from the usual ones; this could induce a relative error on the magnification which can be up to 10%. The reflectivity maximum deduced from the calculations is 99.8%.

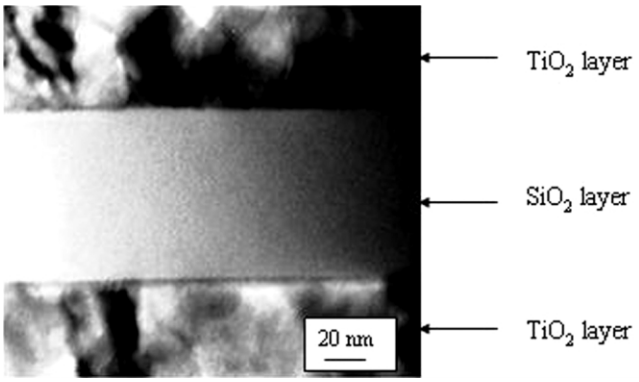

Fig. 4. TEM enlarged image of a cavity shown in Fig. 3. The SiO_2 middle layer is inserted between two TiO_2 layers.

Fig. 6 shows the reflection spectrum of a microcavity with 7 doublets DBRs. The stop band has the same width as the single DBR and a sharp minimum appears at 650 nm. This minimum is related to the half wavelength SiO_2 layer inserted between the DBRs and corresponds to the cavity resonance.

Fig. 7 shows the photoluminescence emission (PL) spectrum of Eu^{3+} ions in the microcavity described above and the spectrum of a single Eu^{3+} doped SiO_2 layer fabricated in the same condition as the microcavity layers but without DBRs. The PL has been excited using the 488 nm blue line of an argon laser (Spectra Physics 2000, excitation power 1 W/cm^2). and is analyzed with a 1 m double monochromator (U1000 Jobin Yvon). A GaAs photomultiplier (RCA31084) coupled to a photon counting system is used as the detector.

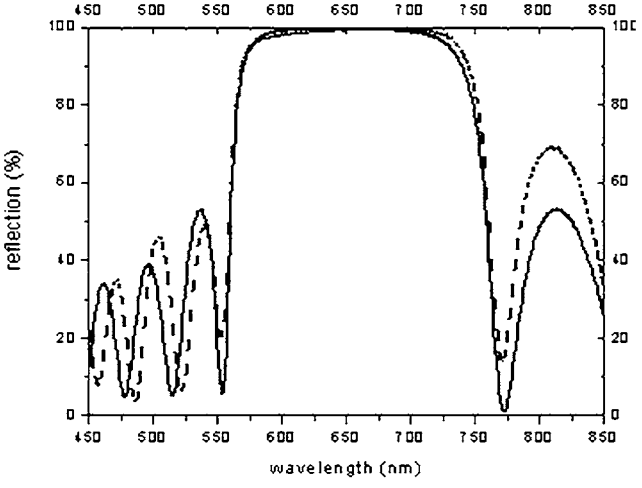

Fig. 5. Reflection spectrum of DBR fabricated with 7 pairs of alternated SiO_2 and TiO_2 layers by the sol–gel process (dashed line) and its simulation (continuous line).

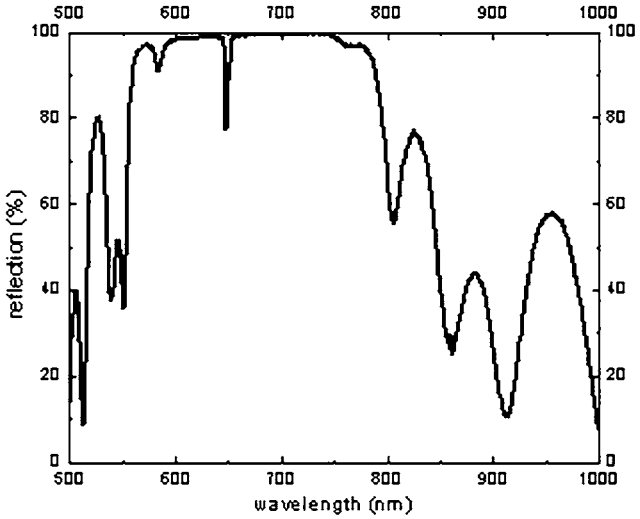

Fig. 6. Reflection spectrum of a microcavity with seven pairs of alternated SiO_2 and TiO_2 layers for each DBR. The stop band is situated between 580 and 780 nm The resonant wavelength is located at 650 nm.

The microcavity emission is detected in an angle of 1° and the Eu^{3+} luminescence in a single SiO_2 layer at an angle of 10°. The Eu^{3+} in SiO_2 layer PL spectrum is centered on 614 nm and its full width at half maximum (FWHM) is 14 nm, this emission corresponds to the $^5D_0 \rightarrow {}^7F_2$ europium transition [15]. The cavity resonance is related to the detection angle as $\lambda_{res} = 2ne\cos(\theta)$, where λ_{res} is the resonance wavelength, n the index of the material, e the thickness of the layer and θ the detection light angle in the material. For a 30° detection angle, the cavity resonance corresponds to the center of the Eu^{3+} PL line. The Eu^{3+} luminescence lineshape is strongly modified in the cavity: the emission at 615 nm is increased by a factor of 20 into the cavity. A sharp line is observed with a FWHM equal to 0.5 nm; this value corresponds to a quality factor of 1200, defined as the ratio $\lambda_{res}/\delta\lambda$ where $\delta\lambda$ is the FWHM of the resonant sharp line. The reflection of each DBR deduced from this value, with the relation $Q = (1+\sqrt{R})^2/(1-R)$, is 99.7% [16]. This value is in fair agreement with the reflection coefficient calculation presented on Fig. 5.

6. Conclusion

In this paper, the sol–gel fabrication of high quality DBRs and microcavities with a Q factor greater than 10^3 is detailed and the optical and structural properties are analyzed. We have shown that an annealing temperature of 900 °C is necessary for the fabrication of such crack-free devices. This annealing treatment opposes stresses in the TiO_2 and SiO_2 layers and allows a stack of more than 60 layers. A short firing time, using a rapid thermal annealing furnace (RTA), is necessary to maintain TiO_2 crystallite sizes small enough in order to keep good optical quality of the layers. DBRs fabricated with this procedure exhibit a reflectivity of 99.7%, deduced from the cavity quality factor. The Eu^{3+} rare earth doping and their luminescence emission behavior

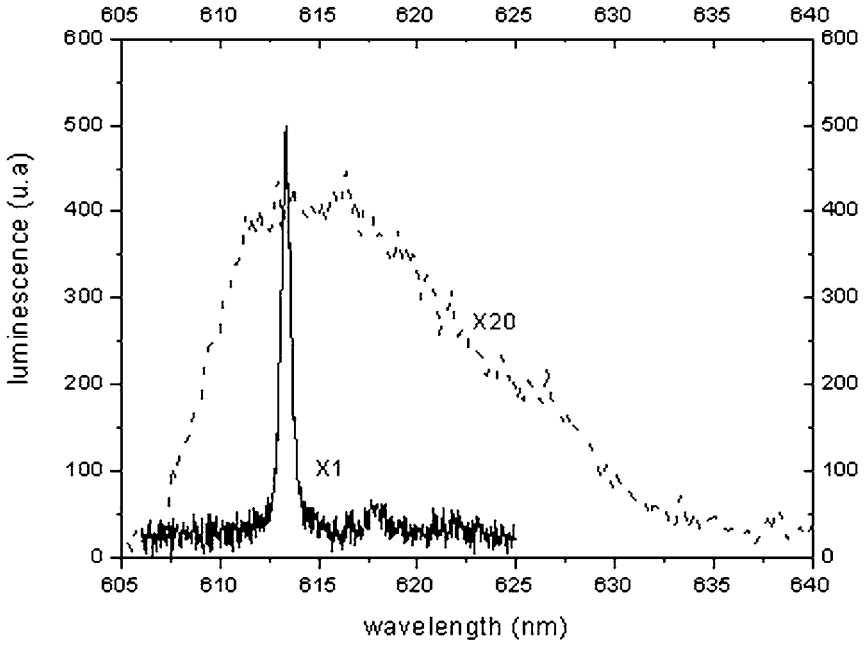

Fig. 7. Luminescence of a single Eu^{3+} SiO_2 layer on a silicon substrate (dashed line) and of a Eu^{3+} SiO_2 layer inserted in a microcavity with a quality factor of 1200 (continuous line).

study, inside and outside the cavity, have been observed and compared.

Acknowledgments

This work was partly funded by the French Ministry of Research program, 'Processus Dynamique à l'Echelle du Nanomètre'.

References

[1] E.M. Purcell, Phys. Rev. 69 (1946) 681.
[2] H. Benisty, C. Weisbuch, M.A. Ganovich, Physica E2 (1998) 909.
[3] J. Bellessa, S. Rabaste, J.C. Plenet, J. Dumas, J. Mugnier, O. Marty, Appl. Plys. Lett. 79 (2001) 2142.
[4] S. Doeuff, M. Henry, C. Sanchez, J. Livage, J. Non Cryst. Solid 89 (1987) 206.
[5] W.C. Lacourse, K.A. Cerqua, J.E. Hyden, J. Non Cryst. Solid 100 (1988) 471.
[6] G. Yi, M. Sayer, Ceram. Bull. 70 (1991) 1173.
[7] P.A Flinn, D.S. Gardner, W.D. Nix, IEEE Transactions on Electron Devices 689(1987)
[8] S.S. Sengupta, S.M. Park, D.A. Payne, L.H. Allen, J. Appl. Phys. 229 (1998) 12296.
[9] T. Chudoba, N. Shwarzer, F. Richter, Surf. Coat. Technol. 127 (2000) 9.
[10] R.R.A. Syms, J. Non Cryst. Solid 167 (1994) 16.
[11] J.T. Fitch, G. Lucovsky, E. Kobeda, E.A. Irene, J. Vac. Sci. Technol. B 7 (1989) 2.
[12] A. Bathat, J. Bouajaoui, A. Bathat, C. Garapon, B. Jacquier, J. Mugnier, J. Non Cryst. Solid 202 (1996) 16.
[13] C.F. Bohren, D.R. Huffmon, Absorption and Scattering of Light by Small Particles, Wiley-Interscience, NY, 1983.
[14] P. Yeh, A. Yariv, Optical Waves in Crystals: Propagation and Control of Laser Radiation, Wiley-Interscience, NY, 1984.
[15] A. Biswas, C.S. Friend, G.S. Maciel, P.N. Prasad, J. Non Cryst. Solid 261 (2000) 9–14.
[16] H. Benisty, J.M. Gérard, R. Houdré, J. Rarity, C. Weisbuch, Confined Photon System, Springer, Cargèse, 1998.